metals

MDPI

Article

Microstructure, Mechanical Properties and Strengthening Mechanism Analysis in an AlMg5 Aluminium Alloy Processed by ECAP and Subsequent Ageing

Przemysław Snopiński and Mariusz Król *

The Division of Materials Processing Technologies Management and Computer Techniques in Materials Science, Institute of Engineering Materials and Biomaterials, Silesian University of Technology, ul. Konarskiego 18a, 44-100 Gliwice, Poland; przemyslaw.snopinski@polsl.pl

* Correspondence: mariusz.krol@polsl.pl; Tel.: +48-32-2371847

Received: 23 October 2018; Accepted: 16 November 2018; Published: 20 November 2018

Abstract: A coarse-grained microstructure of solution treated AlMg5 aluminium alloy was prepared by equal channel angular pressing through route B_C. Microstructure evolution of the alloy was analysed by using an optical microscope, X-ray diffraction, and EBSD (electron backscatter diffraction). The results reported that grains were refined due to the interactions of shear bands with low-to-moderate grain boundaries, and this structure was transformed into a bimodal after ageing at 180 °C for 4 h. Moreover, the results of the tensile testing showed that the yield strength was increased from 110 to 326 MPa, and the corresponding tensile strength increased from 269 to 395 MPa, maintaining an appropriate elongation of ~18%. After ageing at 180 °C elongation increased to 23% and the sample still kept high yield strength of 255 MPa, which may be associated with the mutual influence of the dislocation density decrease and recrystallization processes.

Keywords: aluminium; structure; EBSD; mechanical properties

1. Introduction

In recent years, various severe plastic deformation techniques (SPD) have been used for producing ultrafine-grained materials (UFG). For instance, equal channel angular pressing (ECAP) [1], repetitive corrugation and straightening (RCS) [2], high-pressure torsion (HPT) [3], cyclic extrusion compression (CEC) [4], and accumulative roll bonding (ARB) [5] have been widely applied to produce fine-grained microstructures. Due to the exceptional properties, such as extremely high strength, UFG metals are very interesting to materials scientists. Among all metals, aluminium alloys are mostly used for fabrication UFG microstructures using severe plastic deformation techniques; it is because good workability of aluminium and low required deformation force. It has been also found that the grain refinement of aluminium can be achieved by the addition of Mg. Magnesium has a high solubility in the aluminium ~17.35 wt.% [6,7]. Additionally, the decomposition rate of supersaturated Al-Mg alloys is very low [8]. Therefore, a great majority of Al-Mg alloys display a single phase solid solution matrix. Furthermore, solute Mg atoms decrease the stacking fault energy (SFE) and progress the work-hardenability of these alloys. Reducing of SFE leads to depression in the rate of dynamic recovery which facilitates the formation of UFG microstructure. Refining the grain size of the aluminium–magnesium alloys down to the ultrafine (<1 μm) and even nanometric scale using severe plastic deformation processes become the most effective yield strength increase strategy [9]. However, this increase is mostly accompanied by a loss of ductility. That research has been associated with limited dislocation activity, and hence the absence of work hardening, leading to mechanical

instability [10]. Generally, the trade-off between high strength and ductility is a common problem of materials scientists. Therefore, over the last decades, material engineers had to choose between high strength or high ductility materials, not both as was required. Currently, the following mechanisms are under investigation as agents to ductility control, i.e., bimodal grain size distribution [11,12] and second phase precipitates [12–16]. Bulk bimodal fine-grained aluminium alloys can be produced by a thermomechanical treatment involving severe plastic deformation, i.e., high-pressure torsion or equal-channel angular pressing, followed by an appropriate thermal annealing/ageing under controlled conditions [17]. Postdeformation processing is often carried out on aluminium alloys, to improve their ductility further. During postdeformation processing, recrystallisation may develop bimodal microstructure. Moreover, in heat treatable alloys, precipitation processes remarkably affect mechanical strength, thus a combination of high mechanical properties and enhanced ductility can be obtained [18].

The present study aims to offer and explore a simple approach, i.e., room temperature equal channel angular pressing (ECAP) combined with post-ECAP ageing, to prepare bulk fine-grained Al-Mg alloy with both high ductility and high strength. In this study, therefore AlMg5 aluminium alloy was subjected to ECAP processing followed by a post-ECAP heat treatment. The specific objective was to investigate the grain structure of ECAP and post-ECAP processed samples. Light microscopy, electron backscatter diffraction (EBSD), and X-ray diffractometer (XRD) were employed to examine the evolution of AlMg5 alloy microstructure after post-ECAP heat treatment.

2. Materials and Methods

The raw material used in this study is AlMg5 alloy having a chemical composition in wt.% given in Table 1. The cast ingot was supplied by an Institute of Non-Ferrous Metals in Skawina. The chemical composition was measured using a SPECTROMAXx arc spark OES metal analyser (SPECTRO Analytical Instruments GmbH, Kleve, Germany) according to the ASTM E716-16 standard. The AlMg5 alloy samples were processed in two schemes (i) solution treatment at 560 °C for 12 h → 2× ECAP at room temperature and (ii) solution treatment at 560 °C for 12 h → 2× ECAP at room temperature-artificial ageing for 4 h at 160/180 °C. Solution heat treatment was followed by water quenching. ECAP process was performed via route Bc, using 80 mm × 19.8 mm rods in a 120° die, which leads to an equivalent imposed strain of 0.6 per pass. Molybdenum disulphide was used as a lubricant in the ECAP tests.

Table 1. Chemical composition of AlMg5 alloy (wt.%).

Al	Mg	Si	Fe	Mn	Ti	Zn	Cu	Residuals
94.26	5.54	0.037	0.079	0.0055	0.004	0.004	0.004	0.0665

The microstructure of initial state material, ECAP and post-ECAP processed was studied through light, scanning and transmission electron microscopy. Polarised light images of the alloy before and after ECAP were acquired using AXIO Observer Image Analyser Microscope. Specimens for the EBSD characterization were made by twin-jet electropolishing in a solution of 30% nitric acid and methanol at 30 °C. The EBSD observations were conducted using a scanning electron microscope Zeiss Supra 65 (Carl Zeiss NTS GmbH, Oberkochen, Germany) equipped with a TSL OIM system operating at 20 kV. The misorientation within neighbouring grains was obtained applying a minimum orientation resolution of 2°. Following every scan, data clean-up methods were applied to ensure that all datum points had a probability of ≥95% and confidence index (CI) values ≥0.1. The step size of 0.2 µm was chosen for all EBSD scans. X-ray diffraction analysis was carried out on the polished sections of the heat treated and ECAP processed samples in a PANalytical X'Pert Pro diffraction system (Malvern Panalytical Ltd., Royston, UK) using CoKα radiation, with wavelength λ = 0.1789 nm. The diffraction data were recorded with a scan rate of 0.005°/s. The diffraction profiles applied for crystalline size and lattice strain calculations contained (111), (200), (220), and (311) reflections.

The dislocation density was calculated based on the Williamson-Hall method by calculating the crystallite size, D, and the microstrain, ε, of specimens from the XRD peak broadening, β using the equation

$$\frac{\beta \cos\theta}{\lambda} = \frac{1}{D} + 2\varepsilon \frac{\sin\theta}{\lambda} \quad (1)$$

where λ is the wavelength of the CoKα radiation, θ is the Bragg angle. Plotting $\beta\cos\theta$ against $\sin\theta$, the values of D and ε were obtained directly from the slope and intercept of the fitted curve.

$$\rho = 2\sqrt{3}\left(\varepsilon^2\right)^{\frac{1}{2}} / (D \cdot b) \quad (2)$$

Vickers micro hardness values (HV) were obtained on a cross-section plane. For every sample, a load of 300 gf was applied with 15 s as a dwell time. Tensile tests were carried out using Zwick Z100 equipment (ZwickRoell GmbH & Co.KG, Ulm, Germany) with a strain rate of 6.7×10^{-4} s^{-1}.

3. Results

3.1. Microstructure

Figure 1 shows the optical micrograph of the solution-treated AlMg5 alloy etched using Barker's reagent and analysed in optical microscope (Zeiss, Oberkochen, Germany) using polarised light. It is visible that a large amount of the intermetallic compounds dissolve within the α-Al matrix, showing that the heat treatment reaches the dissolution temperature of Mg-rich phases. The initial microstructure consists of an equiaxed grain with an average intercept length of ~270 µm.

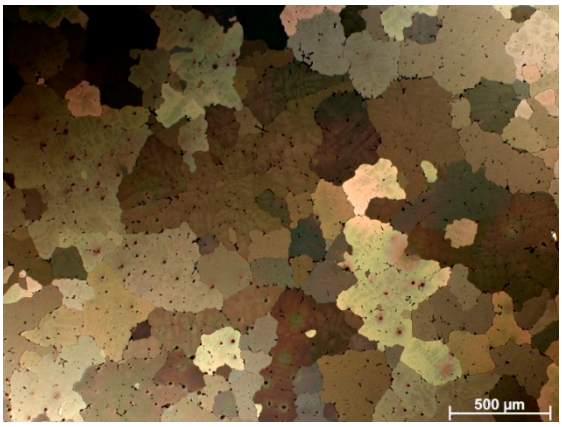

Figure 1. Polarised light microstructure of the AlMg5 alloy in a solution treated state observed under polarised light.

The chemical composition of the precipitates that are present in the microstructure of AlMg5 alloy was examined by energy dispersive spectroscopy (AMETEK BV, Tilburg, The Netherlands). Secondary electron micrograph representing the alloy microstructure in higher magnification is shown in Figure 2. An energy-dispersive X-ray spectroscopy (EDS) chemical composition microanalyses (Table 2) confirmed the presence in the microstructure of AlMg5 alloy of two types of precipitates: Mg_2Si and Al_3Fe distributed at the grain boundary and in grain interiors [7,13,14].

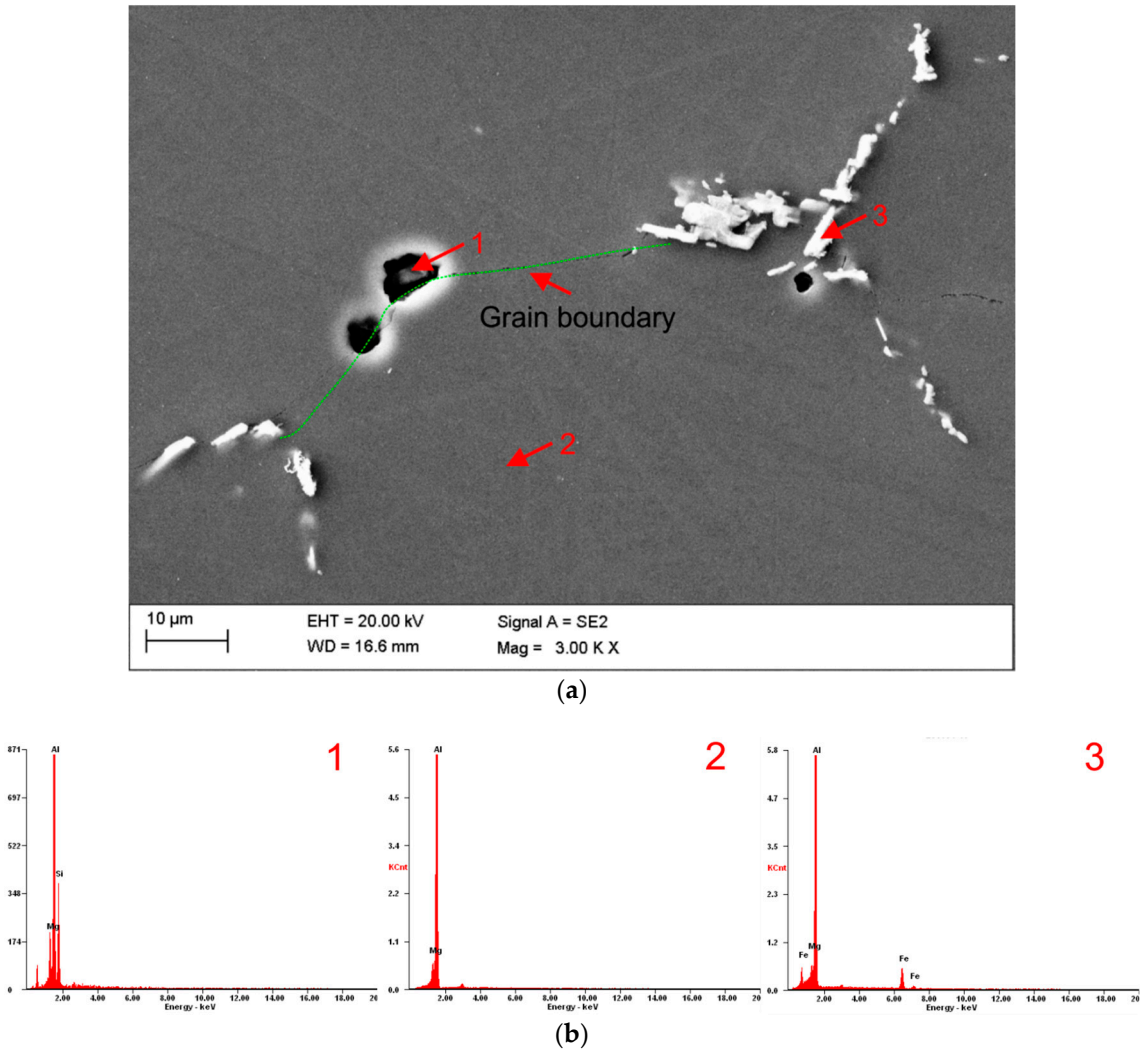

Figure 2. Secondary electron image of a solution-treated AlMg5 alloy (**a**) and corresponding EDS spectra of the analysed phases (**b**).

Table 2. Results of energy-dispersive X-ray spectroscopy (EDS) chemical composition microanalysis.

Element/Line	The Average Concentration of Elements	
	Weight (%)	Atomic (%)
	Point 1	
MgK	4.7	5.3
AlK	57.6	58.1
SiK	37.7	36.6
	Point 2	
MgK	6.9	7.6
AlK	93.1	92.4
	Point 3	
MgK	4.5	5.4
AlK	78.4	85.5
FeK	17.1	9.1

Figure 3a–c shows the microstructure of AlMg5 alloy subjected to the ECAP and post-ECAP ageing treatment. Comparing to the initial microstructure, the processed samples grains are reduced and elongated, some areas of different crystallographic orientation-wavy shear bands forms during ECAP shear deformation. It is evident that these shear bands nucleate on a grain boundary, inducing large

offsets on it. It should be noted that they form on some restricted grain boundaries. One can see also that the grain refinement of the initial microstructure is due to the mutual interactions of these macroscopic shear bands. The observed deformation structures are typical for aluminium alloys subjected to ECAP [19,20]. Elongated coarse grains with parallel DBs are the main features of the microstructures of high 5% > Mg content Al alloys subjected to low strains [21].

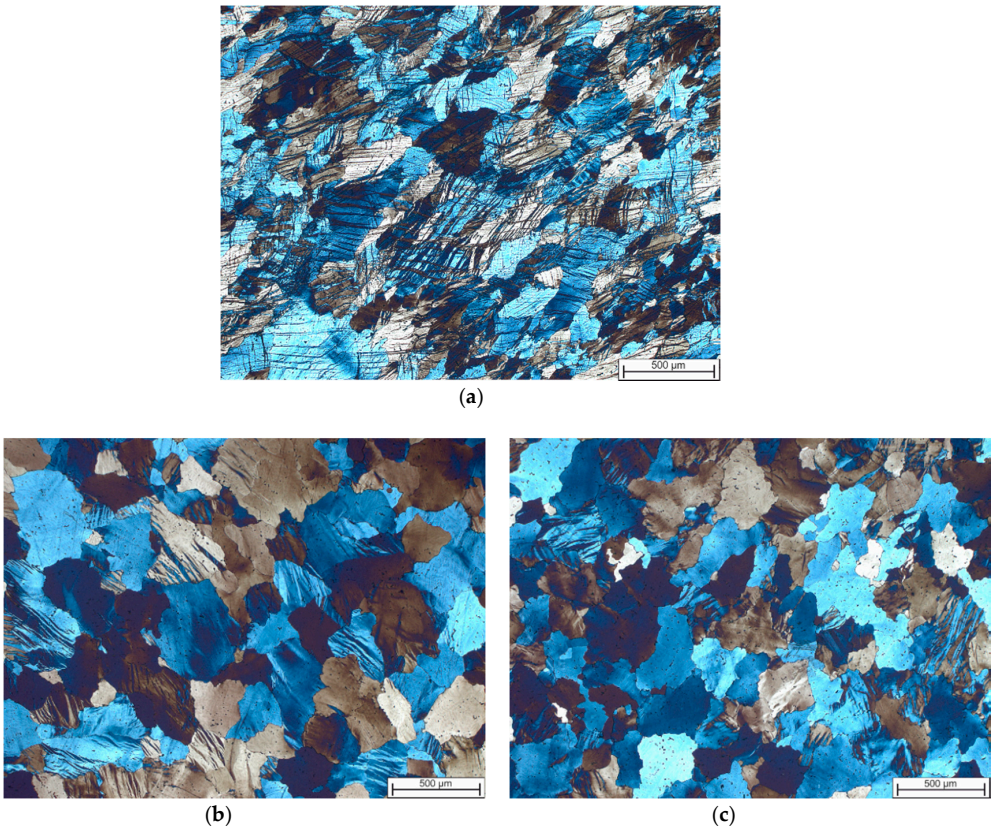

(**a**)

(**b**) (**c**)

Figure 3. Microstructures of the AlMg5 samples (**a**) ST+ ECAP 2×, (**b**) ST + ECAP 2× + ageing 160 °C for 4 h, and (**c**) ST + ECAP 2× + ageing 180 °C for 4 h.

Observation under higher magnification reveals more microstructure detail that occurred after post-ECAP ageing. It is noticeable that the nucleation of brand-new grains occurs (noted as white arrow) at the shear bands (Figure 4b). In the aluminium alloys nucleation occurs by a few mechanisms related to specific microstructural features of the deformed matrix, e.g., particle-stimulated nucleation (PSN), nucleation at shear bands, transition bands (TBs), cube bands, or strain-induced boundary migration (SIBM) [22].

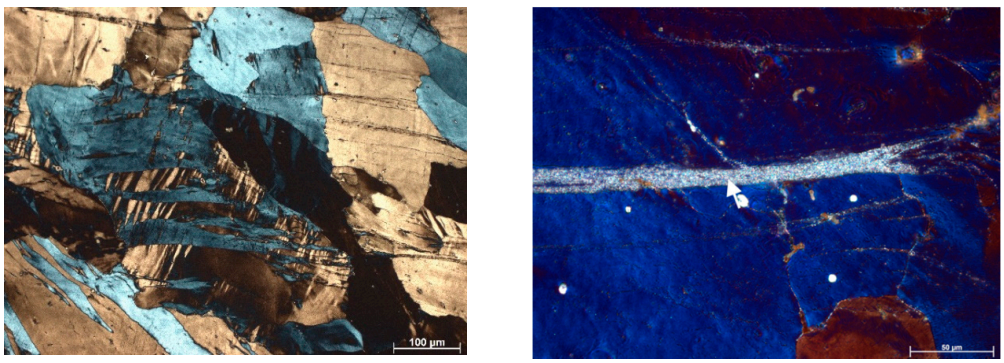

(**a**) (**b**)

Figure 4. Microstructures of the AlMg5 samples (**a**) ST + ECAP 2× +ageing 160 °C for 4 h, (**b**) ST + ECAP 2× + ageing 180 °C for 4 h.

The EBSD colour-coded orientation maps of the AlMg5 alloy in a different condition presented in Figure 5a,b clearly show that the grain refinement cycle proceeds within an ECAP shear deformity. The visible green lines signify high angle grain boundaries (HAGBs) possessing misorientation angle >15°, while red ones match to low angle grain boundaries (LAGBs) with misorientation angle <15°. The coarse grains of solution treated AlMg5 alloy (Figure 1) are subdivided by smooth dislocation boundaries (Figure 5a). Deformation is highly heterogeneous and the shear bands are the main feature of the deformed structure. It is worth to note that most of the subgrains have relatively similar colours based on the unit triangle, and the shear bands have mainly low angle misorientations. Furthermore, in the microstructure subgrains exhibiting an equiaxed shape with an average size of a few microns are also visible. These subgrains are separated by high-angle misorientations above 15°. HAGBs structures are resulted from the continued subdivision of some deformation bands [19]. It is clearly visible that the microstructure of the sample aged at higher (180 °C) temperature differs from the previous one. The shear band boundaries consist of fine recrystallised grains, having a high angle misorientation (Figure 5b). The low angle grain boundaries turn into the high angle boundary misorientation due recrystallisation process [23,24] and therefore the microstructure consists of both elongated with low-to-moderate misorientation angles and equiaxed grains having high angle misorientations. It is believed that the formation of such a bimodal structure is due to the reduced dynamic recovery rate resulting from the high level of Mg solutes [25].

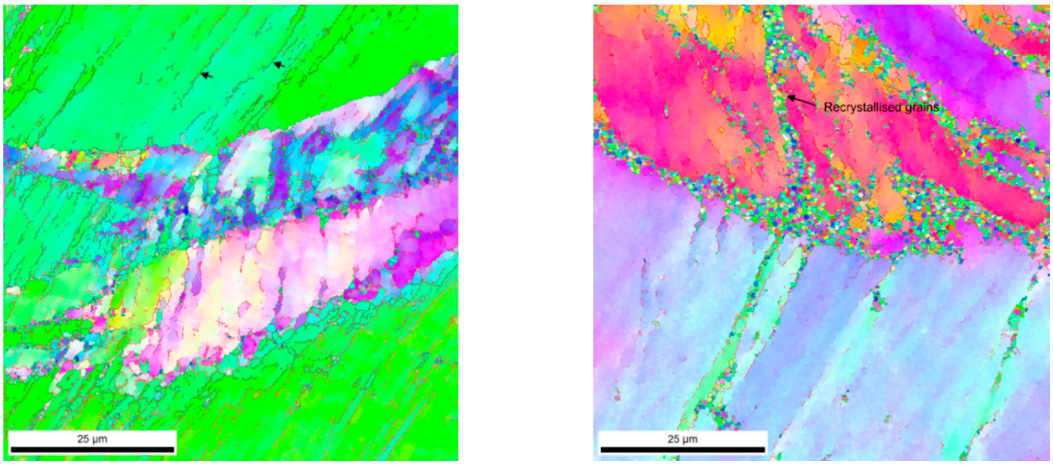

(**a**) (**b**)

Figure 5. Electron backscatter diffraction (EBSD) IPF (Inverse Pole Figure) maps achieved from the centre region of the specimens (cross-section view) (**a**) ST + ECAP 2× + ageing 160 °C for 4 h and (**b**) ST + ECAP 2× + ageing 180 °C for 4 h.

Figure 6a,b shows the fractions (as a percentage) of grain boundaries plotted as a function of the boundary misorientation angle for ST (solution treated) and ECAPed AlMg5 samples aged at 160 and 180 °C. These two graphs express the evolution of microstructure with increasing temperature. In the example aged at 160 °C (Figure 6a) fraction of low angle grain boundaries dominates f_{LAGB} = 59% with the relevant average misorientation Θ_{av} = 19.3°. In the sample aged at 180 °C the misorientation distribution is changes to higher values of angle, and the fraction of the LAGBs decreases to f_{LAGB} = 18% with the relevant average misorientation Θ_{av} = 35.2° (Figure 6b). The increase in the fraction of high angle boundaries, due to the recrystallisation after postdeformation heat treatment in an Al-Mg alloy was also observed by Singh et al. [26] and Zolotorevskiy et al. [27].

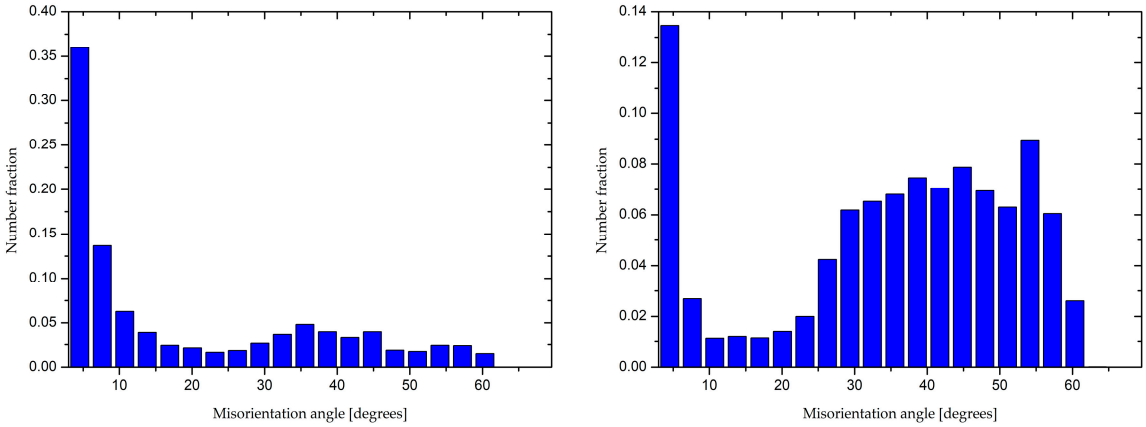

Figure 6. Misorientation angle distribution of the AlMg5 alloy samples (**a**) ST + ECAP 2× + ageing 160 °C for 4 h and (**b**) ST + ECAP 2× + ageing 180 °C for 4 h.

Figure 7a,b shows the histograms of the grain size distribution of the ECAP processed samples subjected to post-ECAP ageing. The average grain size was reduced from ~270 µm in the solution treated state to ~3.22 µm (aged at 160 °C) and ~2.33 µm (aged at 180 °C). The lower grain size in the sample aged at 180 °C is due to the presence of small recrystallised grains at the shear bands.

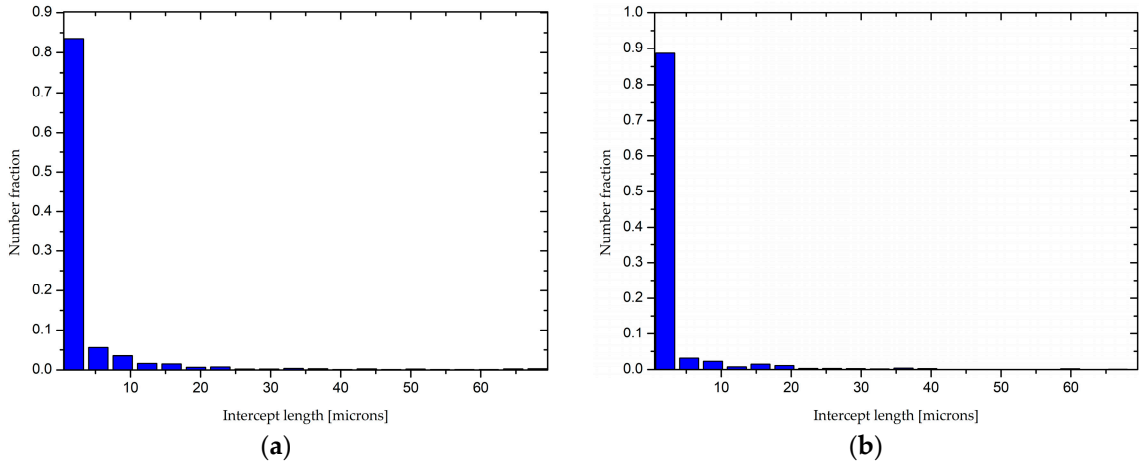

Figure 7. Grain size distribution of the AlMg5 alloy samples (**a**) ST + ECAP 2× + ageing 160 °C for 4 h and (**b**) ST + ECAP 2× + ageing 180 °C for 4 h.

The XRD patterns of ECAP processed and post-ECAP aged samples shown in Figure 8. As shown in the XRD patterns, the (111), (200), (220), and (311) reflections were found corresponding with the cubic close-packed Al structure. The observed differences in relative peak intensity indicate changes in the texture of the alloy during post-ECAP-ageing. The peak broadening is a due presence of lattice defects, which are dislocations and grain boundaries.

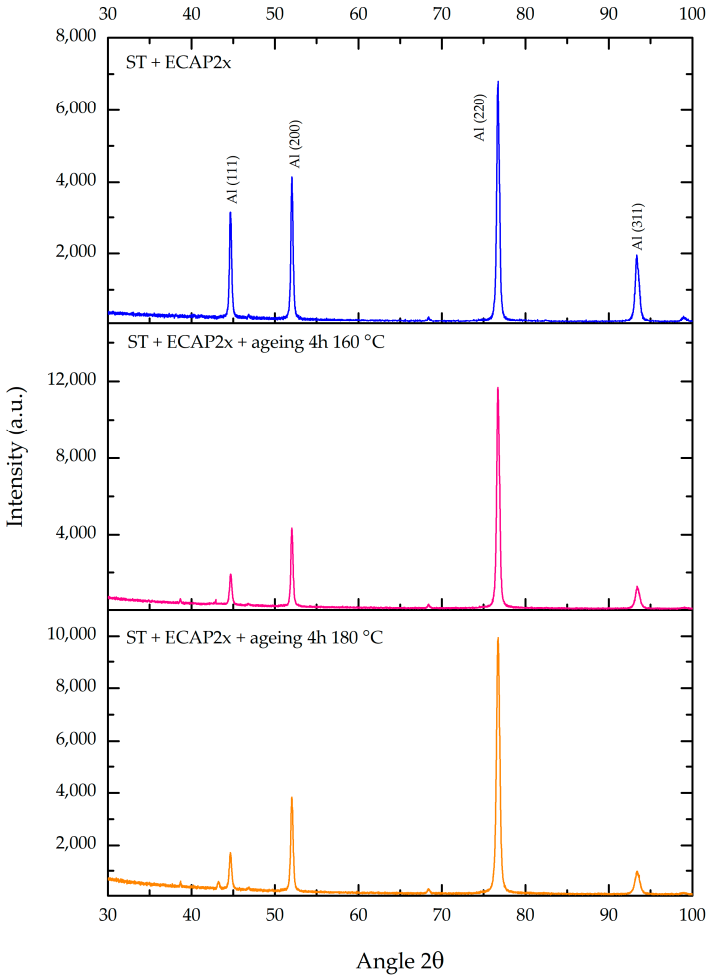

Figure 8. X-ray diffraction pattern of the AlMg5 specimens.

The microstrain and crystallite size calculations results are shown in Table 3. The lattice microstrain of the post-ECAP aged sample decrease from about 1.25 × 10^{-3} to 9.21 × 10^{-4} after 4 h ageing at 160 °C. The crystallite size of the sample after 2 ECAP passes reaches the value of about 60 nm and increases slightly to 67 and 83 nm after ageing at 160 and 180 °C, correspondingly. It is also evident that dislocation density reduces from ~0.224 ×10^{14} m^{-2} (in the as ECAPed condition) to ~0.134 × 10^{14} m^{-2} after artificial ageing.

Table 3. Summarised results of the XRD analysis.

Condition	Lattice Strain, *e*	Crystallite Size, *d* (nm)	Dislocation Density *ρ*
ST + ECAP 2×	1.25·× 10^{-3}	60	0.224·× 10^{14} m^{-2}
ST + ECAP 2× + ageing 160 °C for 4 h	1.16·× 10^{-3}	67	0.209·× 10^{14} m^{-2}
ST + ECAP 2× + ageing 180 °C for 4 h	9.21·× 10^{-4}	83	0.134·×·10^{14} m^{-2}

ST—solution treatment.

3.2. Mechanical Properties

Tensile test curves of the solution treated, as ECAPed and post-ECAP aged samples are shown in Figure 9. Flow serrations during tensile deformation (DSA effect—dynamic strain aging) of as ECAPed and post-ECAP aged samples are visible on the engineering stress-engineering strain curves. The DSA effect is microscopically controlled by dynamic interactions between the mobile dislocations and diffusing solute atoms [28]. In a solution treated sample A type of flow serrations are observed;

whereas in the post-ECAP aged samples, the combination of A and B types of flow serrations takes place.

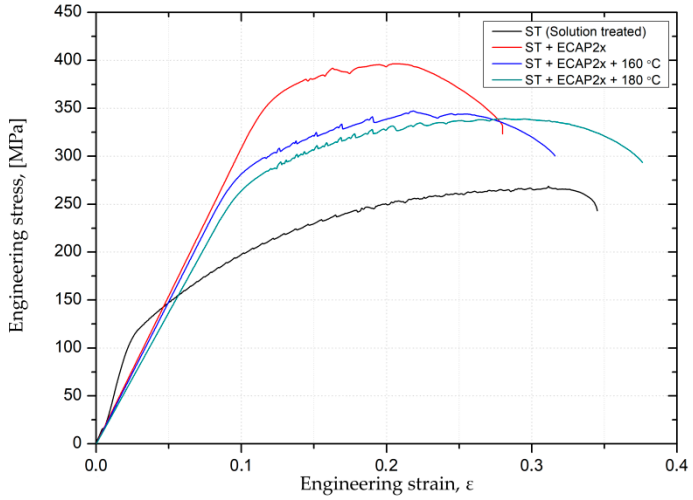

Figure 9. Comparison of engineering stress-engineering strain curves for the AlMg5 alloy subjected to different types of treatments.

The accumulation of structural defects and grain refinement achieved by applying large plastic strains exerts a considerable influence on mechanical properties of the AlMg5 alloy (Table 4). As a result, the strain hardening takes place and consequentially mechanical properties increase. The ultimate tensile strength of AlMg5 alloy after ECAP process (2ECAP passes) increased from 269 to 395 MPa (about 53% increase). Typical reported values of the tensile strength for similar—not the same alloys, are in the range of 340 to 510 (MPa) [20,29] and those values depend on the processing history as well as the starting condition. Artificial ageing of as ECAPed samples led to a mechanical property drop. Tensile strength has decreased by about 13% in comparison with the as deformed state, to ~340 MPa.

ECAP shear deformation also has a meaningful influence on the ductility. It is visible from the tensile test curves that ECAP processing has led to tensile elongation decrease from 28 to 18%. Post-ECAP heat treatment had a beneficial influence on the ductility, which is increased from 18 to 23%.

Artificial ageing of ECAP processed samples increases plasticity due to the annihilation of dislocations and activation of recovery processes. Dislocation climb and cross slip during post-ECAP aged samples, cause to break down the Lomer-Cottrell locks and dislocation release from pins. The as ECAP processed sample microstructure with high dislocation density is replaced by the lower dislocation density microstructure. Moreover, during artificial ageing recrystallisation occurs (Figure 5b). The high uniform ductility of the AlMg5 alloy is mainly ascribed to the strong work hardening that resulted from the bimodal grain structure, a high Mg solute content and the DSA effect [20]. On the other hand, precipitates that could form during ageing may pin-up dislocations and simultaneously increasing the strength. Therefore, both high strength and ductility of the material subjected to the combination of processes are obtained.

Table 4. Mechanical properties of AlMg5 alloy before and after ECAP processing.

The Property	ST	ST + ECAP 2×	ST + ECAP 2× + 160 °C 4 h	ST + ECAP 2× + 180 °C 4 h
Ultimate Tensile Strength (MPa)	269 ± 1	395 ± 2	345 ± 2	340 ± 1
Yield Strength (MPa)	110 ± 1	326 ± 2	271 ± 2	255 ± 1
Elongation, %	28 ± 1	18 ± 1	21 ± 1	23 ± 2
Hardness, HV0.3	73 ± 1	136 ± 1	123 ± 1	120 ± 1

Figure 10 shows the fracture surfaces of the as-built horizontal and vertical tensile test samples. The solution treated specimen (Figure 10a,b) exhibits obvious necking before failure, and the fracture

surface of has various dimple sizes. ECAP processing increased the amount of non-uniformities (Figure 10c,d). It is also visible, that ECAP processed samples fractured under an angle of approximately 41 to 43° to the load axis; hence almost in the direction of maximum shear stresses (Figure 10c–h). The change from necking fracture in the solution treated state to shear that the plasticity slightly decreases as a result of severe plastic deformation. The fracture surfaces exhibit ductile fracture behaviour, with some typical transgranular dimples. It is worth to mention that the elongation to fracture is quite large, see table 3.

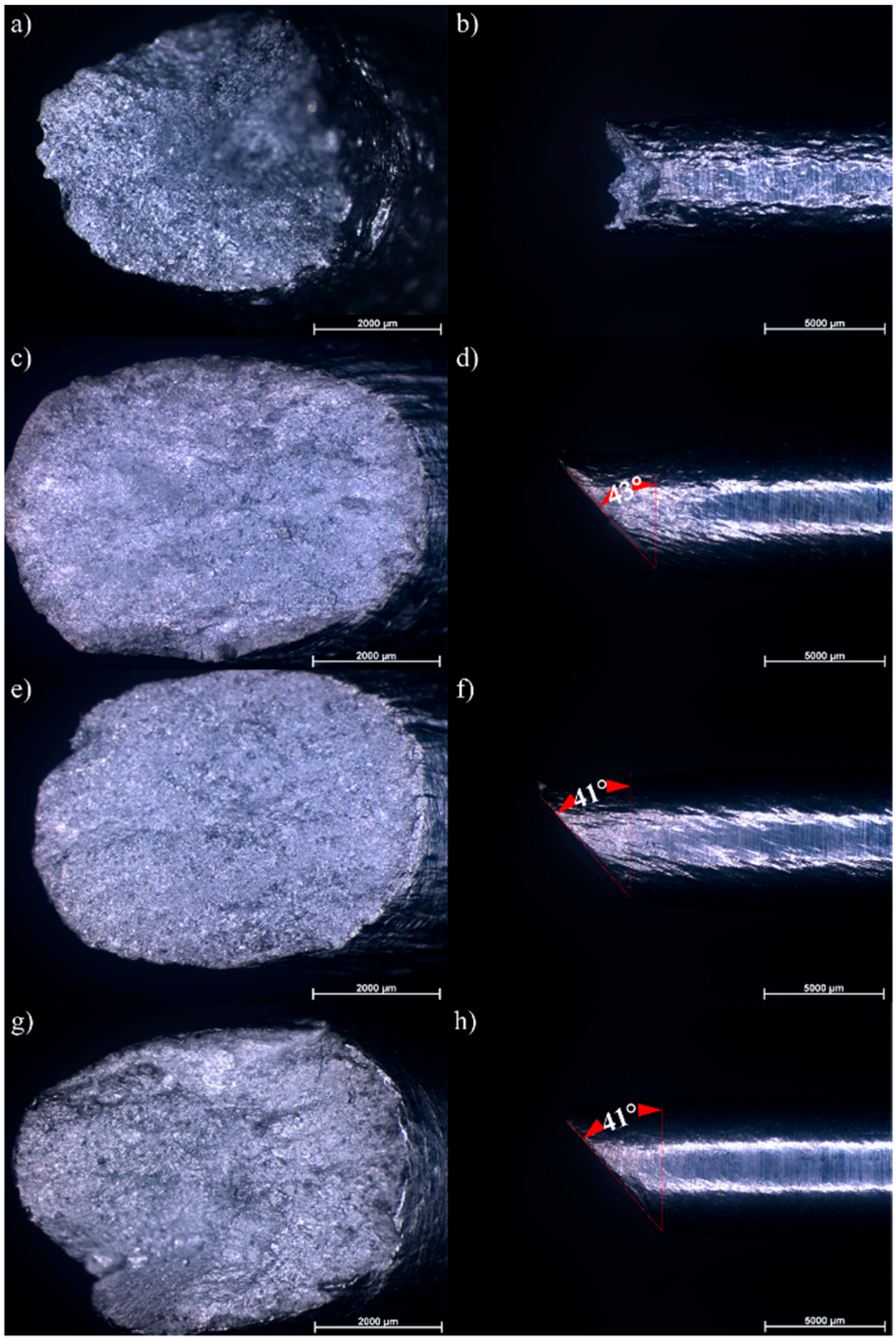

Figure 10. Fracture surfaces of as-built vertical and horizontal samples: (**a**) and (**b**) solution-treated (ST); (**c**) and (**d**) ST + ECAP 2×; (**e**) and (**f**) ST + ECAP 2× + ageing 160 °C for 4 h; and (**g**) and (**h**) ST + ECAP 2× + ageing 180 °C for 4 h.

3.3. Strengthening Mechanism Analysis

It is obvious that ECAP processing significantly affects the grain structure and the mechanical properties as well as the post-ECAP ageing treatment. The strengthening mechanisms are discussed in this section with the aim to evaluate the relationship between the obtained microstructure and yield strength. Taking into account that strength contributions are linearly additive, the total YS of the AlMg5 alloy can be expressed as

$$\sigma_{0.2} = \sigma_0 + \sigma_{SS} + \sigma_{GB} + \sigma_D, \tag{3}$$

where $\sigma_{0.2}$ is the yield strength, σ_0 is the is the friction stress, i.e., the resistance stress for the material with sufficiently large grains and low dislocation density (σ_0 = 10 MPa), σ_{SS} is the solid solution strengthening, σ_{GB} is the grain boundary strengthening—due the grain refinement, σ_D is the dislocation strengthening.

Solid solution strengthening (σ_{SS}) is controlled by the magnesium in solid solution and can be expressed as follows

$$\sigma_{SS} = HC^n, \tag{4}$$

where C is the concentration of Mg in solid solution and n and H are constants equal to 1.19 and 13.3 MPa/(wt.%). In this calculation we neglect precipitation strengthening because all Mg was dissolved during annealing and no particles precipitate during ageing. Substituting C = 5.54 wt.% and the values of constants, the value finally estimates σ_{SS} = 102 MPa.

The vast majority of the alloying elements (i.e., Si and Fe) contribute to the formation of intermetallic phases, as confirmed by EDS chemical composition microanalysis. In the case of the AlMg5 alloy, the Si and Fe atoms are few ppm in concentration, and they do not contribute to alloy strengthening significantly.

The most important and visible from the microstructural point of view consequence of ECAP process is the grain refinement. The obtained refined microstructure shows improved YS which the Hall-Petch equation may explain the increase as below.

$$\sigma_{GB} = k_y d^{-0.5}, \tag{5}$$

where: k_y is the Hall-Petch coefficient -0.13, d is an average grain size obtained by EBSD investigation: ~3.22 μm sample aged at 160 °C for 4 h and ~2.32 μm sample aged at 180 °C for 4 h. The calculated contribution to the Yield strength reaches the value of σ_{GB} = ~85 MPa.

In the work-hardened materials dislocations mutually interacts and impede their motion. Therefore, increasing the dislocation density, the yield strength increases. The importance of dislocation strengthening may be expressed as follows.

$$\sigma_D = M\alpha Gb\rho^{1/2}, \tag{6}$$

where σ_D is the strength increment from dislocation strengthening, α is a constant 0.24, G is the shear modulus 24 GPa, b is magnitude of Burgers vector in aluminum is 0.286 nm, M is a Taylor factor neglecting the crystallographic texture effects as the first approximation (M = 3.06 for polycrystalline aluminium), and ρ is a dislocation density calculated using a Williamson-Hall method. The overall contribution due the stored dislocations reaches a value of σ_D = 69 MPa sample aged at 160 °C and 62 MPa sample aged at 180 °C.

The significant increment in the mechanical properties of the AlMg5 alloy is the sum of four strengthening mechanisms, i.e., dislocation strengthening, solution strengthening and grain size strengthening. Solution strengthening arises from the elastic distortions performed by substitutional Mg atoms in the aluminium matrix, while specimens were subjected to solution treatment prior ECAP. Dislocation strengthening is due to the dislocation generation, motion and interactions of dislocations with grain boundaries. After ECAP process grains were divided, and subgrains with LAGBs were

formed, thus more barriers to dislocation movement were introduced. Therefore, a significant increase in the YS was obtained for the AlMg5 alloy (Table 5).

Table 5. Summary of the calculated strengthening mechanism.

Condition	σ_0 (MPa)	$\Delta\sigma_{Mg}$ (MPa)	$\Delta\sigma_{GB}$ (MPa)	$\Delta\sigma_D$ (MPa)	Calculated Yield Strength (MPa)	Measured Yield Strength (MPa)
ST + ECAP 2× + ageing 160 °C for 4 h	10	102	84	69	265	271
ST + ECAP 2× + ageing 180 °C for 4 h			85	62	259	255

4. Conclusions

Microstructural development and mechanical characteristics of the solution treated AlMg5 aluminium alloy prepared by ECAP at ambient temperature, and following ageing treatment was studied in the present work. The main findings can be summarised as follows.

Coarse grains of as solution treated AlMg5 alloy sample becomes elongated and were gradually replaced after ECAP process into microstructure with wavy shear bands in the grain interiors.

Grain refinement through ECAP may be associated with the frequent evolution of deformation zones containing various LAGBs. By increasing the ageing temperature nucleation of fine grains was observed and those LAGBs are gradually transformed to the HAGBs. The f_{LABs} was decreased from ~59% after ageing at 160 °C to ~18% after ageing at 180 °C for 4 h. Also, the average misorientation angle was increased from 19.3° to 35.2°, respectively.

The ECAP operation causes a rise in the yield strength and hardness up to three times in analysed materials. The corresponding ultimate tensile strength increased from 269 to 395 MPa. Nevertheless, the elongation was lowered from ~28% prior ECAP to ~18% after 2 ECAP passes. The very high strength of as ECAP processed AlMg5 alloy is due to the dislocation and grain size strengthening.

After post-ECAP ageing treatment at 160 °C and 180 °C for 4 h, the sample prepared by 2 ECAP passes obtained larger elongation of ~21% and 23%, and still kept a high yield strength of ~270 MPa and tensile strength of ~326 MPa.

The tensile fractographies of the AlMg5 alloy samples are dominated by the dimple-induced transgranular fracture. Furthermore, the dimples are related mainly to the coarse constituents.

The observed combination of the lattice microstrain decrease, increase in crystallite size and nucleation of fine grains at the shear bands are one of the key factors influencing the ductility increase of the post-ECAP aged samples.

The relationships are described that captures the character of the strengthening mechanism and calculated values of the strengthening contributions to the yield stressfit the experimental results well.

A good compromise of mechanical properties could be achieved by a proper combination of the ECAP and ageing processes.

Author Contributions: P.S. and M.K. conceived and designed the experiments; P.S. performed the experiments, contributed reagents, materials; P.S. and M.K. analyzed the data; M.K. analysis tools; P.S. and M.K. wrote the paper.

Funding: This research received no external funding.

Acknowledgments: This work was supported by the Ministry of Science and Higher Education of Poland as the statutory financial grant of the Faculty of Mechanical Engineering, Silesian University of Technology.

Conflicts of Interest: The authors declare no conflict of interest.

References

1. Ciemiorek, M.; Chrominski, W.; Olejnik, L.; Lewandowska, M. Evaluation of mechanical properties and anisotropy of ultrafine grained 1050 aluminum sheets produced by incremental ECAP. *Mater. Des.* **2017**, *130*, 392–402. [CrossRef]
2. Jenix, R.J.; Balasivanandha, P.S.; Padmanabhan, K.A. On the influence of repetitive corrugation and straightening on the microstructure and mechanical properties of AA 8090 Al-Li alloy. *Arch. Civ. Mech. Eng.* **2018**, *18*, 280–290.

3. Liu, Y.; Liu, M.; Chen, X.; Cao, Y.; Roven, H.J.; Murashkin, M.; Valiev, R.Z.; Zhou, H. Effect of Mg on microstructure and mechanical properties of Al–Mg alloys produced by high pressure torsion. *Scr. Mater.* **2019**, *159*, 137–141. [CrossRef]
4. Wang, Q.; Mu, Y.; Lin, J.; Zhang, L.; Roven, H.J. Strengthening and toughening mechanisms of an ultrafine grained Mg-Gd-Y-Zr alloy processed by cyclic extrusion and compression. *Mater. Sci. Eng. A* **2017**, *699*, 26–30. [CrossRef]
5. Morovvati, M.R.; Dariani, B.M. The effect of annealing on the formability of aluminum 1200 after accumulative roll bonding. *J. Manuf. Process.* **2017**, *30*, 241–245. [CrossRef]
6. Totten, G.E.; MacKenzie, D.S. *Handbook of Aluminum: Physical Metallurgy and Processes*; Marcel Dekker: New York, NY, USA, 2003.
7. Snopiński, P.; Król, M.; Tański, T.; Krupińska, B. Effect of cooling rate on microstructural development in alloy ALMG9. *J. Therm. Anal. Calorim.* **2018**, *133*, 379–390. [CrossRef]
8. Straumal, B.B.; Baretzky, B.; Mazilkin, A.A.; Phillipp, F.; Kogtenkova, O.A.; Volkov, M.N.; Valiev, R.Z. Formation of nanograined structure and decomposition of supersaturated solid solution during high pressure torsion of Al–Zn and Al–Mg alloys. *Acta Mater.* **2004**, *52*, 4469–4478. [CrossRef]
9. Duan, Z.C.; Chinh, N.Q.; Xu, C.; Langdon, T.G. Developing processing routes for the equal-channel angular pressing of age-hardenable aluminum alloys. *Metall. Mater. Trans. A* **2010**, *41*, 802–809. [CrossRef]
10. Witkin, D.; Lee, Z.; Rodriguez, R.; Nutt, S.; Lavernia, E. Al–Mg alloy engineered with bimodal grain size for high strength and increased ductility. *Scr. Mater.* **2003**, *49*, 297–302. [CrossRef]
11. Wang, T.S.; Zhang, F.C.; Zhang, M.; Lv, B. A novel process to obtain ultrafine-grained low carbon steel with bimodal grain size distribution for potentially improving ductility. *Mater. Sci. Eng. A* **2008**, *485*, 456–460. [CrossRef]
12. Shaeri, M.H.; Salehi, M.T.; Seyyedein, S.H.; Abutalebi, M.R.; Park, J.K. Microstructure and mechanical properties of Al-7075 alloy processed by equal channel angular pressing combined with aging treatment. *Mater. Des.* **2014**, *57*, 250–257. [CrossRef]
13. Tański, T.; Snopiński, P.; Prusik, K.; Sroka, M. The effects of room temperature ECAP and subsequent aging on the structure and properties of the Al-3%Mg aluminium alloy. *Mater. Charact.* **2017**, *133*, 185–195. [CrossRef]
14. Tański, T.; Snopiński, P.; Borek, W. Strength and structure of AlMg3 alloy after ECAP and post-ECAP processing. *Mater. Manuf. Process.* **2017**, *32*, 1368–1374. [CrossRef]
15. Tański, T.; Snopiński, P.; Hilser, O. Microstructure and mechanical properties of two binary Al–Mg alloys deformed using equal channel angular pressing. *Materialwiss. Werkstofftech.* **2017**, *48*, 439–446. [CrossRef]
16. Sroka, M.; Zieliński, A.; Hernas, A.; Kania, Z.; Rozmus, R.; Tański, T.; Śliwa, A. The effect of long-term impact of elevated temperature on changes in the microstructure of Inconel 740H alloy. *Metalurgija* **2017**, *56*, 333–336.
17. Fan, G.J.; Choo, H.; Liaw, P.K.; Lavernia, E.J. Plastic deformation and fracture of ultrafine-grained Al–Mg alloys with a bimodal grain size distribution. *Acta Mater.* **2006**, *54*, 1759–1766. [CrossRef]
18. Kim, W.J.; Chung, C.S.; Ma, D.S.; Hong, S.I.; Kim, H.K. Optimization of strength and ductility of 2024 Al by equal channel angular pressing (ECAP) and post-ECAP aging. *Scr. Mater.* **2003**, *49*, 333–338. [CrossRef]
19. Yang, X.; Wang, D.; Wu, Z.; Yi, J.; Ni, S.; Du, Y.; Song, M. A coupled EBSD/TEM study of the microstructural evolution of multi-axial compressed pure Al and Al–Mg alloy. *Mater. Sci. Eng. A* **2016**, *658*, 16–27. [CrossRef]
20. Zha, M.; Li, Y.; Mathiesen, R.H.; Bjørge, R.; Roven, H.J. High ductility bulk nanostructured Al–Mg binary alloy processed by equal channel angular pressing and inter-pass annealing. *Scr. Mater.* **2015**, *105*, 22–25. [CrossRef]
21. Chen, Y.J.; Chai, Y.C.; Roven, H.J.; Gireesh, S.S.; Yu, Y.D.; Hjelen, J. Microstructure and mechanical properties of Al–xMg alloys processed by room temperature ECAP. *Mater. Sci. Eng. A* **2012**, *545*, 139–147. [CrossRef]
22. Crumbach, M.; Goerdeler, M.; Gottstein, G. Modelling of recrystallisation textures in aluminium alloys: I. Model set-up and integration. *Acta Mater.* **2006**, *54*, 3275–3289. [CrossRef]
23. Duckham, A.; Engler, O.; Knutsen, R.D. Moderation of the recrystallization texture by nucleation at copper-type shear bands in Al-1Mg. *Acta Mater.* **2002**, *50*, 2881–2893. [CrossRef]
24. Zhang, J.X.; Ma, M.; Liu, W.C. Effect of initial grain size on the recrystallization and recrystallization texture of cold-rolled AA 5182 aluminum alloy. *Mater. Sci. Eng. A* **2017**, *690*, 233–243. [CrossRef]

25. Zha, M.; Li, Y.; Mathiesen, R.H.; Bjørge, B.; Roven, H.J. Annealing response of binary Al–7Mg alloy deformed by equal channel angular pressing. *Mater. Sci. Eng. A* **2013**, *586*, 374–381. [CrossRef]
26. Singh, D.; Rao, P.N.; Jayaganthan, R. Effect of deformation temperature on mechanical properties of ultrafine grained Al–Mg alloys processed by rolling. *Mater. Des.* **2013**, *50*, 646–655. [CrossRef]
27. Zolotorevskiy, V.S.; Dobrojinskaja, R.I.; Cheverikin, V.V.; Khamnagdaeva, E.A.; Pozdniakov, A.V.; Levchenko, V.S.; Besogonova, E.S. Evolution of the structure and mechanical properties of sheets of the Al–4.7Mg–0.32Mn–0.21Sc–0.09Zr alloy due to deformation accumulated upon rolling. *Phys. Met. Metall.* **2016**, *117*, 1163–1169. [CrossRef]
28. Zhao, S.; Meng, C.; Mao, F.; Hu, W.; Gottstein, G. Influence of severe plastic deformation on dynamic strain aging of ultrafine grained Al–Mg alloys. *Acta Mater.* **2014**, *76*, 54–67. [CrossRef]
29. Vinogradov, A.; Nagasaki, S.; Patlan, V.; Kitagawa, K.; Kawazoe, M. Fatigue properties of 5056 Al–Mg alloy produced by equal-channel angular pressing. *Nanostruct. Mater.* **1999**, *11*, 925–934. [CrossRef]